Power Electronic Systems
Laboratory

Proceedings of the 2nd IEEE International Power Electronics and Application Conference and Exposition (PEAC 2018), Shenzhen, China, November 4-7, 2018

New PCB Winding "Snake-Core" Matrix Transformer for Ultra-Compact Wide DC Input Voltage Range Hybrid B+DCM Resonant Server Power Supply

G. Knabben,
J. Schäfer,
L. Peluso,
J. W. Kolar,
M. Kasper,
G. Deboy

Eidgenössische Technische Hochschule Zürich
Swiss Federal Institute of Technology Zurich

New PCB Winding "Snake-Core" Matrix Transformer for Ultra-Compact Wide DC Input Voltage Range Hybrid B+DCM Resonant Server Power Supply

G. C. Knabben, J. Schäfer, L. Peluso, J. W. Kolar
Power Electronic Systems Laboratory, ETH Zurich
Zurich, Switzerland
knabben@lem.ee.ethz.ch

M. J. Kasper, G. Deboy
Infineon Technologies
Villach, Austria

***Abstract*—Given the demand for higher power density, higher efficiency and lower realization cost solutions in data centers, dc-dc converters using PCB winding magnetics and resonant operation have been intensively studied in literature. In this paper, a new approach for $300\,\mathrm{V}$-$430\,\mathrm{V}$ dc input and $12\,\mathrm{V}$ dc output server power supplies is proposed, which is based on a series resonant converter topology using a synergy between boundary and discontinuous conduction mode operation, whereby low peak-to-average ratio transformer current waveforms, soft-switching throughout the full power range and tight regulation of the output voltage for a wide input voltage range are achieved. Furthermore, a PCB winding "snake-core" matrix transformer is introduced, which provides only a single path for the magnetic flux and therefore ensures an equal flux linkage and/or induced voltage of the parallel-connected secondary windings despite possible geometric PCB layout asymmetries. This approach avoids the emergence of circulating currents between parallel-connected secondary windings and guarantees at the same time equal secondary-side voltages in power supplies with multiple isolated outputs. Thus, a higher degree of freedom in the design of the primary windings of PCB winding-integrated transformers is achieved, whereby the design of these transformers is considerably simplified.**

***Index Terms*—Resonant Converter, Boundary and Discontinuous Conduction Modes, PCB Winding-Integrated Transformer, Circulating Currents.**

I. Introduction

As the electricity consumption of data centers is steeply increasing worldwide due to the high data volume being processed in the cloud during the last years [1], server supply systems with high efficiency, high power density and low realization costs are in demand. Despite recent efforts on changing the common $12\,\mathrm{V}$ data center bus architecture to $48\,\mathrm{V}$, or to even $400\,\mathrm{V}$, and to integrate the final voltage regulator module (VRM) in the CPU motherboards [2], the majority of solutions still relies on two-stage $180\,\mathrm{V}$-$270\,\mathrm{V}$ ac input to $12\,\mathrm{V}$ dc output power conversion at a typical power density up to $50\,\mathrm{W/in^3}$ [3]. For next generation ac-dc converters, an increase in power density to at least $100\,\mathrm{W/in^3}$ is demanded while still being able to handle the typically wide input voltage range and the large output currents of such converter systems. Therefore, the dc-dc converter stage of future server power supplies should comply with the exemplary set of specifications given in **Table I.**

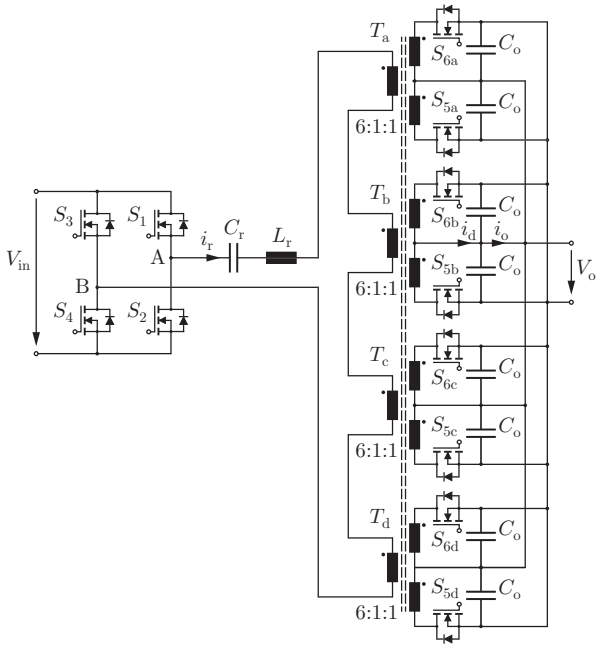

Fig. 1. Power circuit of a resonant $300\,\mathrm{V}$-$430\,\mathrm{V}$ input, $12\,\mathrm{V}$ output, $3\,\mathrm{kW}$ dc-dc converter operating in boundary and discontinuous conduction mode (B+DCM), capable of equally splitting the large output current by means of a matrix transformer with one single magnetic core path for the magnetic flux circulation.

Although numerous galvanically isolated dc-dc converter concepts for data centers have been proposed in literature [4]–[7], the most promising approaches take advantage of winding-integrated PCB magnetics and resonant converter topologies, achieving exceptional performances in terms of power density ($900\,\mathrm{W/in^3}$) and efficiency ($97.6\,\%$) in particular designs [8]. By series connecting the transformer's primary windings and parallel connecting the corresponding secondary windings, i.e. by employing a so-called matrix transformer (cf. **Fig. 1**), the large output current can be distributed among several secondary windings, whereby significantly reduced copper losses and improved PCB heat extraction are achieved. However, in state-of-the-art PCB winding matrix transformers, the different magnetic subcircuits T_x (x=[a,b,c,d] cf. **Fig. 1**) are magnetically connected in parallel, whereby multiple paths for the magnetic

978-1-5386-6054-6/18/$31.00

TABLE I
SERVER POWER SUPPLY DC-DC CONVERTER DESIGN SPECIFICATIONS AND EXPECTED PERFORMANCE

Output Power (P_o)	$3\,\mathrm{kW}$
Output Voltage (V_o)	$12\,\mathrm{V}$
Input Voltage (V_in)	$300\,\mathrm{V}$-$430\,\mathrm{V}$
Volume	$< 100\,\mathrm{cm}^3$
Power Density	$> 490\,\mathrm{W/in}^3$
Efficiency	$> 97\,\%$

flux exist, possibly resulting in asymmetric flux distribution within the transformer and/or asymmetric flux linkages of the transformer windings. Thus, if the primary windings are not perfectly symmetrically arranged, different flux values are present in the transformer T_x and therefore different voltages are induced in each secondary winding, leading to undesired inter-winding circulating currents and thus increased conduction losses. In addition to the challenging transformer design, known resonant converter systems are typically designed for constant input voltage and therefore are not capable to regulate the output voltage for the specified wide input voltage range.

In order to extend the allowable input voltage range of these dc-dc converter concepts and to overcome the transformer's circulating currents issue, this paper proposes the use of a full-bridge LC resonant converter operated either in boundary or discontinuous conduction mode (B+DCM) and employing a PCB winding matrix transformer whose core ensures equal magnetic flux linkages of all windings. In **Section II**, the operation principle of the proposed converter is explained, which shows sinusoidal current waveforms for high load conditions and soft-switching of all semiconductors over a wide power range. **Section III** introduces the new transformer structure and compares it with concepts shown in literature. Experimental results validating the proposed magnetic core concept are presented in **Section IV**. **Section V** summarizes the main findings of the paper.

II. PROPOSED CONVERTER TOPOLOGY AND OPERATION PRINCIPLE

In order to achieve the required $300\,\mathrm{V}$-$430\,\mathrm{V}$ to $12\,\mathrm{V}$ dc-dc power conversion and provide galvanic isolation, a transformer with 24:1 turns ratio which is able to handle $250\,\mathrm{A}$ of converter dc output current is required. As shown in **Fig. 1,** the utilization of four identical sub-transformers T_x (x=[a,b,c,d]), with primary windings connected in series and single-turn secondary windings connected in parallel, allows for splitting the output current and accordingly reduces the losses in the secondary windings. Synchronous rectifiers with power MOSFETs ($S_{5\mathrm{x}}$, $S_{6\mathrm{x}}$, $\mathrm{x} = [\mathrm{a,b,c,d}]$) which are directly connected to output capacitors (C_o) are chosen in order to avoid diode voltage drops on the secondary side that would result in significant conduction losses due to the large output current. In addition, inductive filters in the current path should be avoided for the same reason. Since the transformer secondary windings are directly connected to capacitive filters (voltage source characteristic), the series-connected primary windings must be excited by a current source, whose waveform should be sinusoidal in order to minimize the harmonic content of the transformer current i_r and therefore the resulting high frequency conduction losses in the magnetic components as well. These sinusoidal currents can be generated employing a LC resonant tank with rectangular voltage excitation by the primary-side full-bridge (S_1-S_4).

The output power of this converter can be regulated by either changing the switching frequency and/or the duty cycle of the exciting primary-side voltage v_AB. Hence, using the aforementioned control parameters, two main operating modes can be achieved, i.e. continuous conduction mode (CCM) where the current flows continuously in the inductor L_r and almost sinusoidal current waveforms are generated, and alternatively discontinuous conduction mode (DCM) which allows for operating the converter with a constant switching frequency for all power values and yields partially synchronized primary- and secondary-side gate drive signals. However, both operating modes have significant drawbacks, as in CCM the gate drive signals are not synchronized, whereby a complex control scheme for the synchronous rectifier switches is required (additional current measurement circuitry), and in DCM, the peak-to-average ratio of i_d is very large, resulting in increased current harmonics and therefore conduction losses as well. Consequently, the converter should be operated at the boundary between the two operating modes (BCM), as then the benefits of CCM and DCM are combined and drawbacks are circumvented. However, similar to the CCM, the BCM requires very high values of switching frequency f_s for low output power values, which is why below a certain output power level, the DCM is used in combination with zero votlage switching (ZVS) in order to reduce switching losses. Hence, similar to solutions used in flyback-based microinverters [9,10], a synergy between BCM and DCM is proposed as suitable and efficient control method for this converter.

For low input voltages and full power, where the largest currents are processed, the converter works in BCM with almost sinusoidal currents and the lowest peak-to-average ratios (cf. **Fig. 2(a)**). The switching losses are minimized, as for S_3, S_4, $S_{5\mathrm{x}}$, $S_{6\mathrm{x}}$ ZVS and for S_1, S_2 zero current switching (ZCS) are achieved. ZVS in S_1 and S_2 can also be achieved by placing an air gap in the transformer core, which increases the magnetizing current and supports the commutation. For high input voltages and/or low power, f_s needs to be increased so that the output voltage v_o stays constant. Nevertheless, i_d still has very low peak-to-average ratio and the gate signals are still synchronized, as shown in **Fig. 2(b)**. At a certain value, the switching frequency is not increased any more as high frequency effects (e.g. skin effect losses) start to play a role. Therefore, DCM is now applied and the duty cycle is reduced while keeping f_s constant (cf. **Fig. 2(c)**). The peak-to-average ratio of i_d is now larger but the absolute values are relatively low as the converter operates in light load. Consequently, the triangular shape of the waveforms will not contribute significantly to the conduction losses, but will still help in achieving ZVS transitions, which are more important in light load conditions as capacitive switching losses are more expressive.

In summary, using this simple control strategy, roughly sinusoidally shaped transformer currents are achieved while

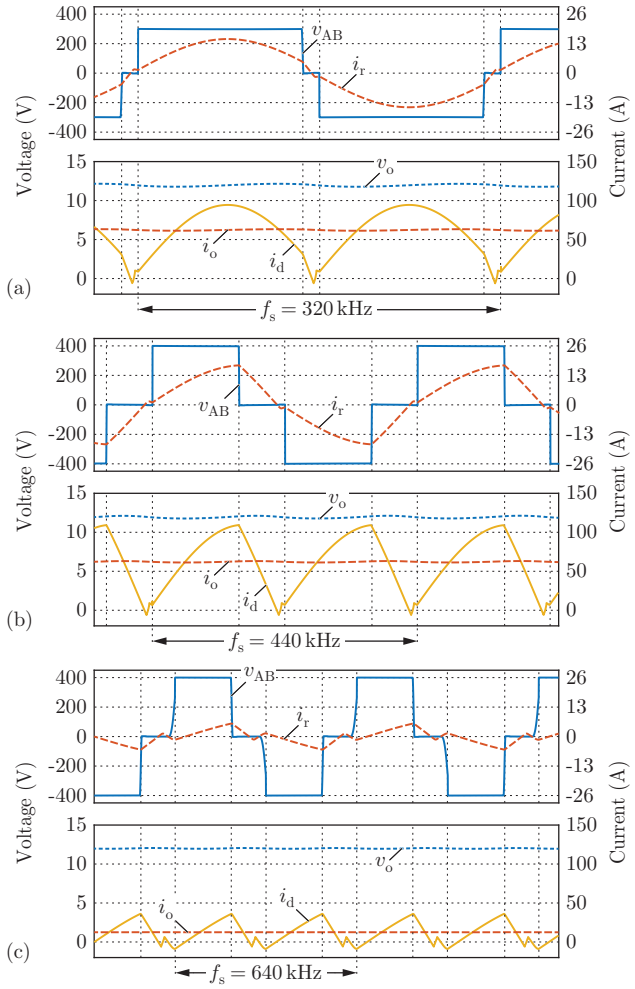

Fig. 2. Main waveforms of the converter shown in **Fig. 1** for different operating points (V_{in}/P_o): (a) 300 V/3 kW, (b) 400 V/3 kW and (c) 400 V/600 W.

at the same time excessive switching losses are avoided. However, in order to reduce the conduction losses in the transformer even further, a sophisticated transformer design is required, which ensures a homogeneous current distribution among the secondary windings and prevents circulating currents within the transformer. In the following section, such transformer concept is proposed and analysed in detail.

III. Transformer Concept and Analysis

The proposed transformer is implemented in a 4-layer PCB, where the middle layers are assigned to the series-connected primary turns and the top and bottom layers to the secondary windings, respectively. In order to minimize the termination losses and to increase the power density of the converter, the switches of the synchronous rectifiers (S_{5x}, S_{6x}) and the output capacitors (C_o) are directly integrated into the secondary windings, as schematically depicted in **Fig. 3(a)**. The coplanar arrangement of the primary- and secondary-side currents theoretically cancels the vertical magnetic field components within the windings and leads to very low ac-to-dc resistance ratios. Even for high switching frequencies, a current distribution close to the dc current density is achieved. The PCB copper thickness (105 µm) is chosen to be smaller than the skin depths (137 µm-94 µm) of the switching frequency operation range (320 kHz-640 kHz), in order to avoid skin effects due to horizontal magnetic field components.

In state-of-the-art PCB winding matrix transformers, the required close magnetic coupling of the primary and the secondary windings is usually achieved using core geometries similar to **Fig. 3(b)**, where two ferrite plates are placed above and underneath the PCB windings in order to magnetically connect the (four) core legs. Hence, the previously mentioned parallel connection of the four magnetic sub-circuits results. Assuming open-circuits in all secondary windings and a symmetric core geometry, the structure can be represented by the reluctance model of **Fig. 3(c)**. $N_p i_p$ refers to the generated magnetomotive force (MMF) of the primary windings, ϕ to the magnetic flux flowing in each leg and $\Re$ to the reluctances of the magnetic paths. If $N_{p1} = N_{p2} = N_{p3} = N_{p4}$, the symmetry of the transformer yields the same flux linkage in each leg, whereby in each secondary winding identical voltages are induced. However, due to PCB routing limitations, some turns of the primary windings might be incomplete, as for instance indicated by the dashed lines in **Fig. 3(a)**, creating discrepancies between the MMF generated in each leg and therefore inducing different voltages in the secondary windings.

In order to better understand the statement, a winding arrangement according to $N_{p1} > N_{p2} = N_{p4} > N_{p3}$ is assumed. In this particular case, the MMF generated within the legs 2 and 4 are equal (same current and same number of turns) and the reluctance model of **Fig. 3(c)** can be replaced with the circuit shown in **Fig. 4(a)**, where the legs with the same MMF are connected in parallel. The circuit can be further simplified to the one shown in **Fig. 4(b)**, where it can be seen that if N_{p1} is larger than N_{p3}, $\phi_1 > \phi_3$ applies. Basically, the fluxes can be equated as $\phi_1 > \phi_2 = \phi_4 > \phi_3$ and therefore different voltages are induced in the secondary windings N_{s1} and N_{s3} (single turns), according to $v_{ind} = -d\phi/dt$. As all secondary windings are connected in parallel, the different induced voltages create circulating currents among the windings (cf. **Fig. 4(c)**), which affect the transformer conduction losses.

Aiming to overcome the aforementioned issue, a new core design named as "snake-core" is proposed, where the top and the bottom core plates are divided into two pieces in such a way that the four magnetic sub-circuits T_x are connected in series, whereby only one path for the magnetic flux is provided (cf. **Fig. 3(d)**). The equivalent reluctance model is shown in **Fig. 3(e)** and is similar to the magnetic circuit of **Fig. 3(c)**, however unequal flux splitting in the circuit nodes is now impossible as only a single magnetic path is provided. Hence, $\phi_1 = \phi_2 = \phi_3 = \phi_4$ always applies, leading to equal induced voltages in all secondary windings and therefore no circulating currents. The snake-core transformer also benefits power supplies with several isolated outputs, as each secondary winding inherently experiences the same flux linkage. Consequently, identical output voltages are induced. The design of such transformer is straightforward and will not be shown in this paper, as it follows well-known equations for designing high-frequency magnetics in power electronics [11,12].

In order to validate the operation of the proposed transformer design, finite element simulations were performed

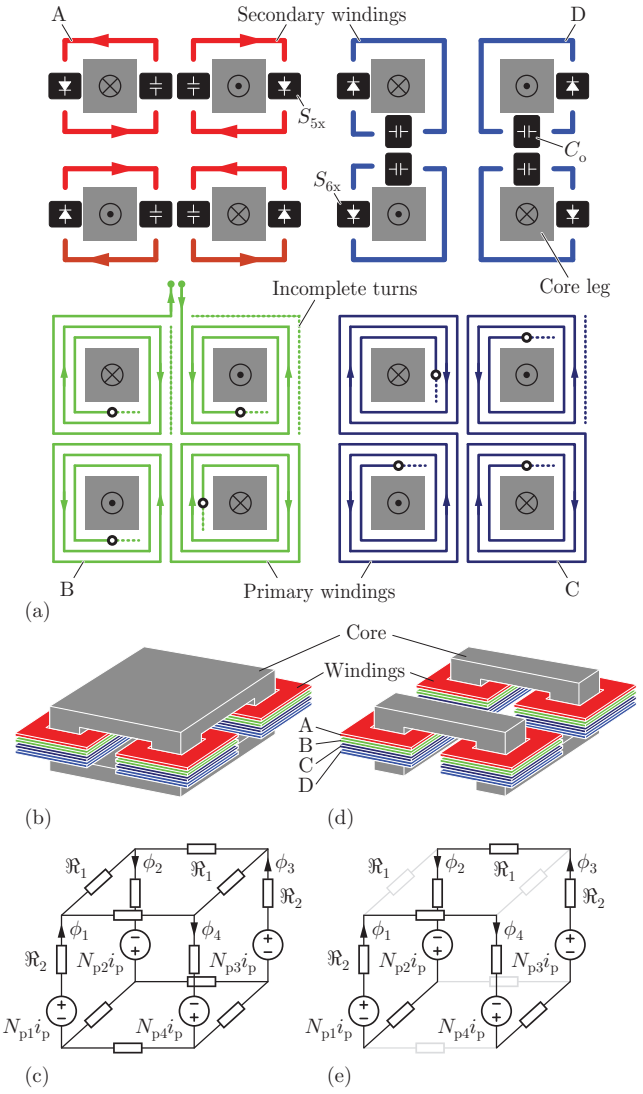

Fig. 3. **(a)** Schematics of the proposed 4-layer PCB winding matrix transformer with the middle layers (B,C) dedicated to the series-connected primary windings and the top (A) and bottom (D) layers implementing the parallel-connected secondary windings. The switches S_{5x} and S_{6x}, as well as the dc-link capacitors C_o, are directly integrated into the windings for power density reasons. **(b)** State-of-the-art core arrangement solution whose magnetic circuit **(c)** shows the possibility of unequal flux distribution across the corners of the cube, causing undesired circulating currents within the secondary windings due to unequal induced voltages. **(d)** Proposed core arrangement to avoid flux splitting and therefore circulating currents; only one path for the magnetic flux is provided, as highlighted in the equivalent magnetic circuit **(e)**.

(cf. **Fig. 5**). Two basic simplifications were done intending to facilitate the construction of the simulation model, i.e. concentric copper rings are utilized for representing the primary turns, and only Secondary 1 is assumed to carry current (zero current in the Secondary 2, as given for a half switching cycle in regular operation). The concentric rings approach does not precisely model the spiral primary winding shape, but still gives a good approximation of the conductions losses and field interactions. By setting zero current in the Secondary 2 and forcing full sinusoidal current in the Secondary 1, the modelling of rectified currents is avoided and a frequency domain FEM simulation can be performed, which requires less data processing and still

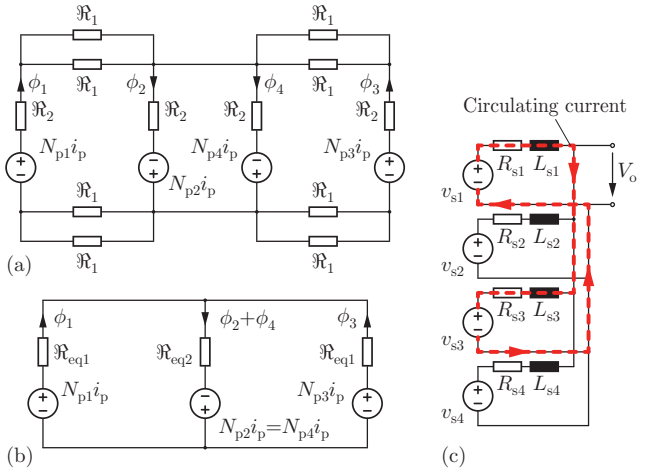

Fig. 4. Equivalent **(a)** and simplified **(b)** circuits of the reluctance model of **Fig. 3(c)** for $N_{p2} = N_{p4}$. **(c)** Circulating currents generated along the parallel connected secondary windings of the transformer due to different induced voltages in the corresponding windings.

provides loss evaluation with mathematical consistency. As shown in **Fig. 5(b)**, due to the coplanar winding arrangement, the vertical components of the magnetic field generated by the primary and secondary windings cancel each other. Consequently, no eddy currents are induced along the windings and a current distribution close to the dc current density is achieved in all windings. The benefits of the coplanar arrangement can also be seen in how the magnetic field is distributed within the windings' vicinity, i.e. the field is almost completely confined in between the PCB layers which reduces radiated electromagnetic interference (cf. **Fig. 5(c)**). The circular shape of the turns is particularly chosen for avoiding sharp corners of the current path which would increase the conduction losses due to the increased current densities around these corners besides the increased winding length. An additional thermal analysis indicates the necessity of heat sinks and air flow for extracting the losses out of the PCB and cooling the windings down to temperatures around 100 °C. Since the primary winding is not modelled with the real spiral shape and Secondary 2 is not conducting current, the thermal simulation does not provide the most accurate result, but was intended to be used for analysing the transformer heat transfer in order to optimize the heat sink positioning. For maximum output power, the calculated and simulated transformer shows approximately 39 W of total losses and a boxed volume of 50 cm^3 (cf. **Table II**), which in terms of efficiency and power density correspond to 98.7 % and 980 $\mathrm{W/in}^3$, respectively. Note that these results are related only to the transformer and do not indicate the full-system performance.

IV. Experimental Results

The primary- and secondary-side winding layout of the proposed PCB winding snake-core matrix transformer is shown in **Fig. 6(a)**, which also includes the secondary-side switches and corresponding gate drive circuits. The core was manufactured by machining off-the-shelf ferrite blocks and plates using a linear precision saw with a diamond blade. Two magnetic core geometries were chosen for comparison purposes: the conventional core with top

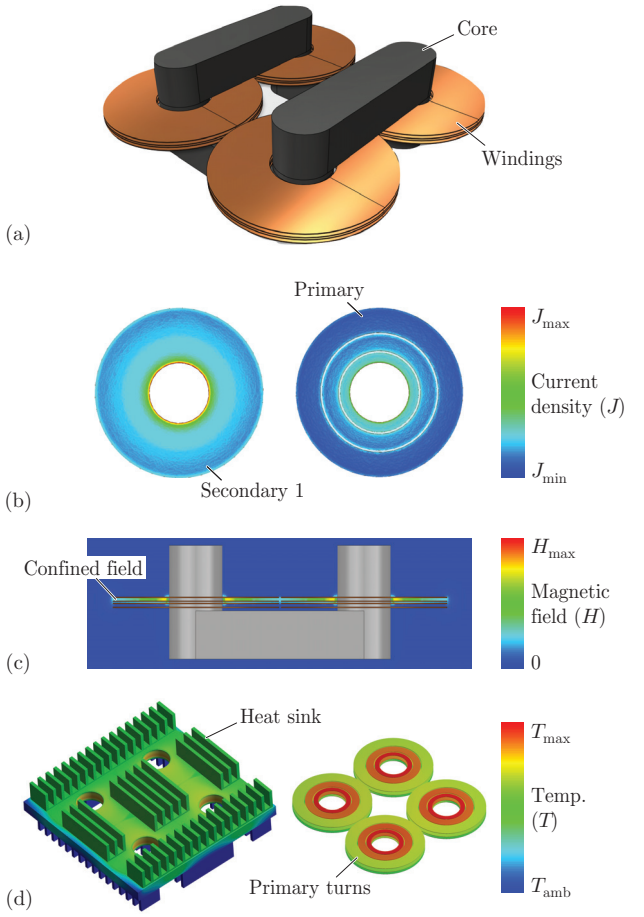

Fig. 5. Transformer construction **(a)**, current density in the series connected primary windings and one secondary winding (Secondary 1) **(b)**, magnetic field in the vicinity of the windings **(c)** and thermal analysis of the transformer **(d)** based on a finite element simulation with 320 kHz sinusoidal current excitation, attached heat sinks and forced convection cooling. For simplifying the simulation without loosing generality, the primary windings were considered as concentric rings and the secondary-side current is assumed to flow in the Secondary 1.

TABLE II
CALCULATED/SIMULATED TRANSFORMER PERFORMANCE

Transformer Performance	Calc. / Sim.
Output Power (P_o)	3 kW
Total Loss (P_{total})	39.1 W / 40.7 W
Copper Loss (P_{Cu})	36.9 W / 39.2 W
Core Loss (P_{Fe})	2.2 W / 1.5 W
Core Material	N49
Switching Frequency (f_s)	320 kHz
Max. Temperature	100 °C

and bottom plates (cf. **Fig. 6(b1)**) and the snake-core (cf. **Fig. 6(b2)**). The snake-core can also be assembled in such a way that larger top and bottom plates are used and therefore lower core losses result (cf. **Fig. 6(b3)**). The fully assembled conventional and snake-core transformer designs are shown in **Figs. 6(c1)** and **6(c2)**, respectively.

A classical open-circuit test was applied to the prototype in order to validate the assumption that equal induced voltages occur in each secondary winding if the snake-core

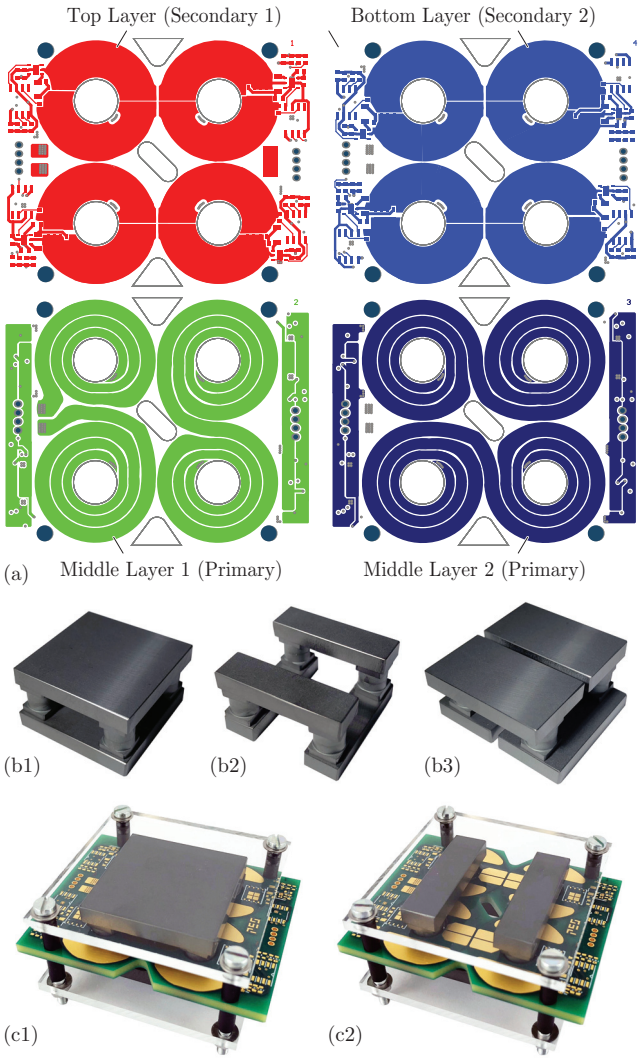

Fig. 6. (a) PCB design of the proposed transformer exhibiting the high- and low-voltage windings implementation. The core can be arranged either in conventional form **(b1)** or can be realized using snake core **(b2,b3)**; the top and bottom bars of the new arrangement might be chosen larger **(b3)** in order to reduce core losses. **(c)** Final transformer assembling, measuring 65 mm x 51 mm x 24 mm (2.6 in x 2.0 in x 0.94 in).

is used. Plugging the series-connected primary windings to a 300 V peak / 320 kHz sinusoidal voltage, the open-circuited secondary winding voltages were measured for the conventional core and the snake-core. The results are shown in **Fig. 7,** in which $v_{p,conv}/v_{p,snake}$, $i_{p,conv}/i_{p,snake}$ and $v_{sx,conv}/v_{sx,snake}$ (x $= [1,2,3,4]$) refer to the transformer primary voltage, primary current and secondary voltages of the conventional and the proposed core, respectively. Despite the efforts in designing the PCB primary windings as symmetric as possible, the measurements reveal that the turns are still not perfectly distributed around the core legs, as different voltages are induced in each secondary winding for the conventional core transformer. However, as expected, the proposed snake-core arrangement provides equal flux distribution among the secondary windings and the induced voltages are the same. This approach not only avoids the emergence of circulating currents among the parallel-connected secondary windings, but also provides a solution for equalizing the voltages in power supplies with several isolated outputs. Thus, regardless a possible

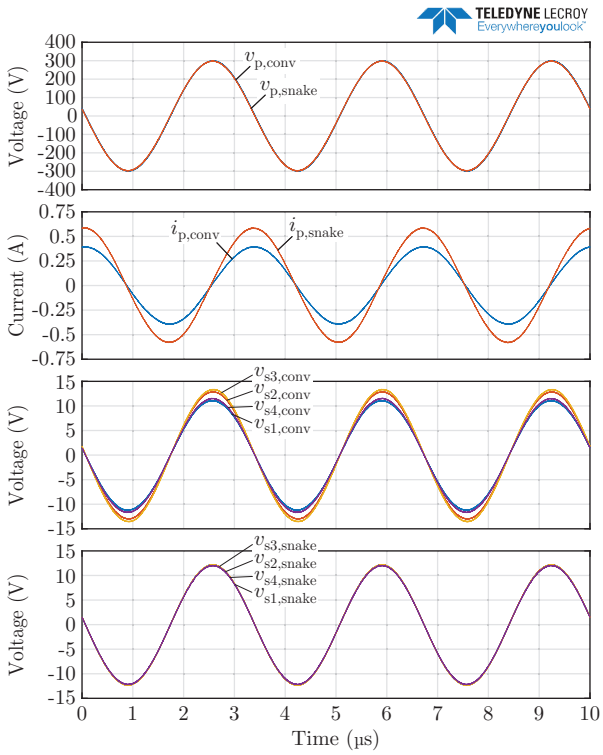

Fig. 7. Open-circuit transformer test using a conventional or the proposed snake-core approach. For the same primary voltage excitation ($v_{p,conv}/v_{p,snake}$), the conventional core transformer (cf. **Fig. 6(c1)**) presents different induced voltages in the secondary windings ($v_{sx,conv}$, x $= [1, 2, 3, 4]$) caused by asymmetries in the primary turns layout, while the proposed snake-core (cf. **Fig. 6(c2)**) keeps the voltages equal ($v_{sx,snake}$). The magnetizing currents ($i_{p,conv}/i_{p,snake}$) of the cores are different due to their different geometries.

asymmetry in the distribution of the primary turns within the transformer, the snake-core ensures identical induced voltages in the secondary windings, whereby not only higher power conversion efficiency results, but also the design of such PCB winding-integrated transformers is considerably simplified.

V. Conclusions

In this paper, a new approach for 300 V-430 V input, 12 V output dc-dc converters is introduced, which allows to fulfil the requirements of next generation data center server power supplies regarding efficiency, power density and costs. The proposed resonant converter concept can tightly regulate the output voltage for wide input voltage variations and large output power fluctuations by combining boundary and discontinuous conduction mode operation. In addition, a low harmonic content of the transformer current is achieved and soft-switching of all power semiconductors is guaranteed. Hence, significantly reduced conduction and switching losses can be obtained. The proposed snake-core PCB winding matrix transformer equally distributes the high output current to several secondary windings and yields very low conduction losses as the coplanar arrangement of the primary and secondary windings minimizes their ac-to-dc resistance ratios. Moreover, the proposed snake-core arrangement due to the single path for the magnetic flux avoids the emergence of circulating currents between parallel-connected secondary windings of the transformer, regardless of possible asymmetries in the layout of the series-connected primary windings around the core legs. It therefore in general facilitates the design of the primary windings of PCB winding matrix transformers and also provides a simple solution for equalizing the secondary-side voltages in power supplies with several isolated outputs.

References

[1] L. Chiaraviglio, F. D'Andreagiovanni, R. Lancellotti, M. Shojafar, N. B. Melazzi, and C. Canali, "An approach to balance maintenance costs and electricity consumption in cloud data centers," *IEEE Trans. on Sustain. Comput.*, pp. 1–1, 2018.

[2] A. Pratt, P. Kumar, and T. V. Aldridge, "Evaluation of 400V dc distribution in telco and data centers to improve energy efficiency," in *Proc. of the 29th IEEE International Telecommunications Energy Conference (INTELEC)*, Rome, Italy, Sep. 2007, pp. 32–39.

[3] Bel Power Solutions & Protection, "TET3000-12-069RA ac-dc front-end power supply," https://goo.gl/tSBhU7, 2018, accessed: 2018-05-30.

[4] K. George and S. Ang, "Topology survey for GaN-based high voltage step-down single-input multi-output dc-dc converter systems," in *Proc. of the 4th IEEE Workshop on Wide Bandgap Power Devices and Applications (WiPDA)*, Fayetteville, USA, Nov. 2016, pp. 32–39.

[5] D. Huang, S. Ji, and F. C. Lee, "Matrix transformer for LLC resonant converters," in *Proc. of the 28th IEEE Applied Power Electronics Conference and Exposition (APEC)*, Long Beach, USA, Mar. 2013, pp. 2078–2083.

[6] F. C. Lee, Q. Li, Z. Liu, Y. Yang, C. Fei, and M. Mu, "Application of GaN devices for 1 kW server power supply with integrated magnetics," *CPSS Trans. on Power Electron. and Applic.*, vol. 1, no. 1, pp. 3–12, Dec. 2016.

[7] M. H. Ahmed, A. Nabih, F. C. Lee, and Q. Li, "High efficiency isolated regulated 48V bus converter with integrated magnetics," in *Proc. of the CPES Power Electronics Conference*, Blacksburg, USA, Apr. 2018.

[8] C. Fei, F. C. Lee, and Q. Li, "High-efficiency high-power-density 380V/12V dc-dc converter with a novel matrix transformer," in *Proc. of the IEEE Applied Power Electronics Conference and Exposition (APEC)*, Tampa, USA, Mar. 2017.

[9] Z. Zhang, M. Chen, W. Chen, and Z. Qian, "Design and analysis of the synchronization control method for bcm/dcm current-mode flyback micro-inverter," in *Proc. of the IEEE Applied Power Electronics Conference and Exposition (APEC)*, Long Beach, USA, Mar. 2013.

[10] G. C. Christidis, A. C. Nanakos, and E. C. Tatakis, "Hybrid discontinuous/boundary conduction mode of flyback microinverter for ac-pv modules," *IEEE Trans. on Power Electron.*, vol. 31, no. 6, pp. 4195–4205, Jun. 2016.

[11] W. Hurley and W. Wölfle, *Transformers and inductors for power electronics: theory, design and applications*, ser. EngineeringPro collection. Wiley, 2013. [Online]. Available: https://books.google.ch/books?id=KAsshIYbQKoC

[12] M. Kazimierczuk, *High-frequency magnetic components*. Wiley, 2013. [Online]. Available: https://books.google.ch/books?id=oPw8AgAAQBAJ